

Hadronic Contributions to the Muon $g - 2$ in Improved Holographic QCD Models

Jin-Yang Shen,^{1,2,*} Wen-Yuan Peng,^{1,2,†} Ling-Yun Dai,^{1,2,‡} and Zhen Fang^{1,2,§}

¹*School of Physics and Electronics,
Hunan University, Changsha 410082, China*

²*Hunan Provincial Key Laboratory of High-Energy Scale Physics and Applications,
Hunan University, Changsha 410082, China*

Abstract

We present a systematic study of the hadronic contributions to the muon anomalous magnetic moment within several infrared-improved AdS/QCD models. The models are constrained by the pion decay constant and the ρ -meson mass and are shown to reproduce phenomenologically reasonable low-energy hadron spectra. Within a unified holographic framework, we evaluate both the leading-order hadronic vacuum polarization contribution and the pseudoscalar-pole contribution to hadronic light-by-light scattering. The holographic predictions for the hadronic vacuum polarization contribution are found to be systematically lower than recent dispersive determinations, and we demonstrate that this discrepancy is closely correlated with an underestimation of the ρ -meson decay constant in the models. We further compute the pion transition form factor and the corresponding pseudoscalar-pole hadronic light-by-light contribution. Although the models yield similar pion mass spectra and reproduce the expected asymptotic behavior, their predictions for the hadronic light-by-light contribution exhibit sizable variations, driven by differences in the transition form factor in the low momentum transfer Q^2 region.

* Jinyang_Shen@hnu.edu.cn

† S240700462@hnu.edu.cn

‡ dailingyun@hnu.edu.cn

§ zhenfang@hnu.edu.cn

I. INTRODUCTION

The anomalous magnetic moment of the muon, $a_\mu = (g - 2)_\mu/2$, constitutes a key precision observable in particle physics and has a long history rooted in early foundational studies [1]. Over the past several decades, sustained experimental efforts have been devoted to continuously improving the measurement precision [2–5]. In 2025, the Fermilab Muon $g - 2$ Collaboration reported its final result based on the complete dataset, achieving an unprecedented precision of 127 parts per billion and establishing an experimental benchmark that is expected to stand for the foreseeable future [6]. Despite this remarkable achievement, the comparison between experiment and the Standard Model prediction has developed into a subtle and evolving situation, with the primary source of tension now residing in the theoretical determination of hadronic contributions [7, 8].

The Standard Model prediction for the muon anomalous magnetic moment receives contributions from three distinct sectors: electromagnetic, electroweak, and hadronic. Among these, the hadronic sector constitutes the dominant source of theoretical uncertainty. It is conventionally decomposed into two components: the hadronic vacuum polarization (HVP) contribution [9–16] and the hadronic light-by-light (HLbL) scattering contribution [17–28]. At present, the evaluation of these hadronic contributions relies on two complementary and increasingly sophisticated theoretical frameworks.

On the one hand, a broad class of phenomenological and theory-driven approaches is employed to constrain both the HVP and HLbL contributions. These include traditional data-driven methods based on dispersion relations, as well as effective field theory descriptions such as resonance chiral theory and vector meson dominance models. In particular, the data-driven approach exploits precise measurements of electron–positron annihilation into hadrons, together with dispersive techniques, to determine the HVP function $\Pi_{\text{em}}^{\text{had}}(Q^2)$ [29]. However, recent high-precision measurements of the $e^+e^- \rightarrow \pi^+\pi^-$ cross section have revealed tensions among different experimental datasets [30]. These discrepancies have propagated into dispersive analyses and have thus far hindered the construction of a single, unified data-driven estimate [8].

On the other hand, first-principle calculation based on lattice QCD provides a systematically improvable and fully nonperturbative alternative that is independent of experimental cross-section data. Recent lattice determinations of the HVP contribution have reached sub-percent precision and can be consistently combined into a lattice average. When these results are supplemented by improved estimates of the HLbL contribution obtained through a synergistic combination of lattice QCD [31] and data-driven constraints [32], the resulting Standard Model prediction becomes compatible with the experimental measurement of the muon $g - 2$ [8, 33, 34]. This evolving theoretical landscape underscores the importance of reconciling lattice QCD results, data-driven determinations, and effective Lagrangian approaches in order to elucidate the origin of the muon $g - 2$ puzzle.

In this context, holographic QCD models inspired by the AdS/CFT correspondence [35–37] provide a valuable framework for exploring nonperturbative hadronic dynamics [38–57]. In recent years, such models have been increasingly applied to the study of the muon anomalous magnetic moment [58–67]. Most existing holographic evaluations of a_μ have been performed within the standard hard-wall or original soft-wall constructions, which offer useful qualitative insights into the structure of hadronic contributions. A distinctive advantage of the holographic approach is the emergence of an infinite tower of vector and axial-vector resonances, allowing for a systematic implementation of QCD short-distance

constraints on correlation functions and form factors. Nevertheless, both the hard-wall and original soft-wall models suffer from well-known quantitative shortcomings. The hard-wall model fails to reproduce linear Regge trajectories, while the original soft-wall framework typically underestimates the decay constants of low-lying vector and axial-vector mesons. Consequently, these models are unable to simultaneously describe key hadronic observables within a single consistent parametrization, leading to non-negligible model-dependent uncertainties in holographic determinations of hadronic contributions to the muon anomalous magnetic moment. This situation motivates a renewed examination of a_μ within improved soft-wall frameworks and a systematic assessment of the stability of holographic predictions under different infrared modifications.

In this work, we revisit the holographic evaluation of the muon anomalous magnetic moment using three infrared-improved soft-wall models [68–70], which incorporate more realistic descriptions of low-energy hadronic dynamics. While holographic approaches to a_μ have been explored in a number of previous studies, most analyses rely on the standard hard-wall or original soft-wall models and typically focus on selected hadronic contributions. Here, we perform a unified calculation of both the leading-order HVP contribution and the pseudoscalar-pole contribution to HLbL scattering within a single holographic setup. The models are constrained to reproduce phenomenologically reasonable meson spectra and decay constants, enabling a systematic investigation of model dependence and a clearer identification of the impact of infrared improvements on holographic predictions for a_μ .

The remainder of this paper is organized as follows. In Sec. II, we introduce the three infrared-improved soft-wall models considered in this work, fix the model parameters by fitting the ground-state ρ -meson mass, the pion mass, and the pion decay constant to their experimental values, and present the resulting hadron mass spectra. In Sec. IV, we compute the leading-order HVP contribution to the muon anomalous magnetic moment in the two-flavor case within these soft-wall frameworks. In Sec. V, we first evaluate the pion two-photon transition form factor and subsequently determine the pseudoscalar-pole contribution to a_μ^{HLbL} for each model. Finally, Sec. VI summarizes our main findings and discusses their implications.

II. THE HOLOGRAPHIC QCD MODELS

A. The infrared-improved soft-wall model (SW1)

In the original soft-wall AdS/QCD model, chiral symmetry breaking cannot be realized in a fully consistent manner [47, 71]. In order to simultaneously and coherently describe linear confinement in low-energy QCD, chiral symmetry breaking, and the resulting meson spectra, an infrared-improved soft-wall AdS/QCD model was proposed in Ref. [68]. The infrared-improved soft-wall model is formulated in an AdS₅ spacetime with the metric ansatz

$$ds^2 = z^{-2} (\eta_{\mu\nu} dx^\mu dx^\nu - dz^2), \quad (1)$$

where $\eta_{\mu\nu} = \text{diag}\{1, -1, -1, -1\}$. The structure of the model is specified by the following five-dimensional action

$$S = \int d^5x \sqrt{g} e^{-\Phi(z)} \text{Tr} \left[|DX|^2 - m_5^2 |X|^2 - \lambda_X |X|^4 - \frac{1}{4g_5^2} (F_L^2 + F_R^2) \right], \quad (2)$$

where the covariant derivative and field strengths are given by

$$D^M X = \partial^M X - iA_L^M X + iX A_R^M, \quad F_{MN}^{L,R} = \partial_M A_N^{L,R} - \partial_N A_M^{L,R} - i[A_M^{L,R}, A_N^{L,R}].$$

The gauge fields are written as $A_{L,R}^M = A_{L,R}^{Ma} t^a$, with the generators normalized according to $\text{Tr}(t^a t^b) = \delta^{ab}/2$. The five-dimensional gauge coupling is fixed by matching to perturbative QCD, yielding $g_5^2 = 12\pi^2/N_c$, where N_c denotes the number of colors [38].

For the dilaton field $\Phi(z)$, the infrared (IR) behavior is required to grow quadratically in order to ensure that the mass spectrum of highly excited mesons exhibits approximately linear Regge trajectories. At the same time, since the introduction of the dilaton field explicitly breaks the original conformal symmetry, $\Phi(z)$ must approach zero in the ultraviolet (UV) limit so that conformality is recovered. To satisfy these UV and IR asymptotic requirements, the dilaton profile in this model is parameterized as

$$\Phi(z) = \mu_g^2 z^2 - \frac{\lambda_g^4 \mu_g^4 z^4}{(1 + \mu_g^2 z^2)^3}. \quad (3)$$

The bulk scalar field can be decomposed as

$$X(x, z) = \left(\frac{\chi(z)}{2} + S(x, z) \right) e^{2i\pi(x, z)}, \quad (4)$$

where $\pi(x, z) = \pi^a(x, z)t^a$ denotes the pseudoscalar meson field and $S(x, z)$ represents the scalar meson field. The vacuum expectation value (VEV) of the bulk scalar field is assumed to take the form

$$\langle X \rangle = \frac{\chi(z)}{2} I_2, \quad (5)$$

with I_2 the 2×2 identity matrix. The scalar VEV $\chi(z)$ satisfies the asymptotic behaviors

$$\chi(z \rightarrow 0) = m_q \zeta z + \frac{\sigma}{\zeta} z^3, \quad \chi(z \rightarrow \infty) = v_q z, \quad (6)$$

where m_q denotes the current quark mass, σ is the chiral condensate, ζ is a normalization constant fixed to be $\zeta = \sqrt{3}/(2\pi)$ (and is taken to have this value throughout this work), and v_q is a constant parameter characterizing the energy scale of dynamically generated spontaneous chiral symmetry breaking. To satisfy the above ultraviolet and infrared asymptotic conditions simultaneously, the scalar vacuum profile is parameterized as

$$\chi(z) = \frac{Az + Bz^3}{1 + Cz^2}, \quad (7)$$

with $A = m_q \zeta$, $B = \sigma/\zeta + m_q \zeta C$, $C = \mu_c^2/\zeta$, and $v_q = B/C$, where the constant parameter μ_c characterizes the QCD confinement scale.

In the action (2), a quartic interaction term for the bulk scalar field is introduced, with a z -dependent coupling chosen to control the ultraviolet and infrared behaviors. In particular, the quartic coupling is required to vanish in the ultraviolet limit, $\lambda_X(z \rightarrow 0) \sim \mu_g^2 z^2 \rightarrow 0$, so that the conformal symmetry of the Lagrangian is preserved near the UV boundary, while in the infrared region it is taken to approach a constant value, $\lambda_X(z \rightarrow \infty) \rightarrow \lambda$, consistent

with the structure of quartic interactions in chiral effective theories of low-energy QCD. Based on these considerations, the quartic coupling is parameterized as

$$\lambda_X(z) = \frac{\mu_g^2 z^2}{1 + \mu_g^2 z^2} \lambda. \quad (8)$$

As demonstrated in Ref. [68], the predictions for the resonance mass spectra are not sensitive to the specific functional form of $\lambda_X(z)$. Accordingly, in the subsequent SW2 and SW3 models, the quartic coupling is treated as a constant parameter, $\lambda_X = \lambda$, without imposing the ultraviolet constraint adopted in the SW1 setup.

B. The improved soft-wall model with 2 flavors (SW2)

An evident limitation of the early soft-wall construction is that the bulk scalar VEV $\chi(z)$, which encodes spontaneous chiral symmetry breaking, is imposed by hand rather than obtained as a genuine solution of its equation of motion (EOM). To remedy this shortcoming, an improved soft-wall AdS/QCD model was proposed in Ref. [69]. The bulk action and background metric in this model are identical to those of the SW1 model introduced above, while the dilaton profile is chosen in the simplest quadratic form

$$\Phi(z) = \mu_g^2 z^2, \quad (9)$$

whose infrared growth ($z \rightarrow \infty$) provides a soft cutoff scale for the action and constitutes a defining feature of the soft-wall framework.

In order to achieve a dynamically consistent realization of chiral symmetry breaking, the improved soft-wall model further introduces a z -dependent five-dimensional mass term for the scalar field. This bulk mass approaches the conventional constant value in the ultraviolet region, ensuring compatibility with the asymptotic freedom of QCD, while increasing toward the infrared, leading to a more natural large- z behavior of the scalar field. In this way, the improved soft-wall model provides a unified and self-consistent description of both confinement and chiral symmetry breaking. The parametrized form of the bulk mass term adopted in this model, and likewise in the subsequent one, is

$$m_5^2(z) = -3 - \mu_c^2 z^2. \quad (10)$$

Starting from the bulk action, the EOM for the scalar VEV $\chi(z)$ can be derived as

$$\chi''(z) - \left(\frac{3}{z} + \Phi'(z) \right) \chi'(z) - \frac{1}{z^2} \left(m_5^2(z) \chi(z) + \frac{\lambda}{2} \chi^3(z) \right) = 0, \quad (11)$$

and the asymptotic behaviors of $\chi(z)$ in this model take the same form as those of the SW1 model.

C. The improved soft-wall model with 2 + 1 flavors (SW3)

In Ref. [70], the SW2 model was generalized to the 2 + 1-flavor case, enabling the calculation of octet meson spectra and their associated decay constants within the improved

soft-wall AdS/QCD framework. This extension makes it possible to realize and systematically investigate the chiral phase transition both at finite baryon chemical potential and for different quark masses in the 2 + 1-flavor case. The action of the improved soft-wall model with 2 + 1 flavors can be written as

$$S = \int d^5x \sqrt{g} e^{-\Phi(z)} \left[\text{Tr} \left(|DX|^2 - m_5^2(z)|X|^2 - \lambda|X|^4 - \frac{1}{4g_5^2}(F_L^2 + F_R^2) \right) - \gamma \text{Re}\{\det X\} \right], \quad (12)$$

where the last term corresponds to the 't Hooft determinant introduced to ensure a correct realization of the chiral transition in the 2 + 1-flavor case. In order to satisfy the required boundary behavior, the dilaton field is parametrized as

$$\Phi(z) = \mu_g^2 z^2 \left(1 - e^{-\frac{1}{4}\mu_g^2 z^2} \right). \quad (13)$$

For 2 + 1 flavors, the VEV of the bulk scalar field takes the form

$$\langle X \rangle = \frac{1}{\sqrt{2}} \begin{pmatrix} \chi_u(z) & 0 & 0 \\ 0 & \chi_d(z) & 0 \\ 0 & 0 & \chi_s(z) \end{pmatrix}, \quad (14)$$

with $\chi_u = \chi_d$. Substituting this scalar VEV into the action, the EOMs for χ_u and χ_s are obtained as

$$\chi_u'' - \left(\frac{3}{z} + \Phi' \right) \chi_u' - \frac{1}{z^2} \left(m_5^2 \chi_u + \lambda \chi_u^3 + \frac{\gamma}{2\sqrt{2}} \chi_u \chi_s \right) = 0, \quad (15)$$

$$\chi_s'' - \left(\frac{3}{z} + \Phi' \right) \chi_s' - \frac{1}{z^2} \left(m_5^2 \chi_s + \lambda \chi_s^3 + \frac{\gamma}{2\sqrt{2}} \chi_u^2 \right) = 0, \quad (16)$$

with the boundary conditions $\chi_{u,s}(0) = \frac{1}{\sqrt{2}} m_{u,s} \zeta$ and $\chi_{u,s}(z \rightarrow \infty) \sim z$.

III. THE MESON SPECTRA AND DECAY CONSTANTS

The parameters of these improved soft-wall models are fixed by matching the calculated ground-state mass of the ρ meson ($m_\rho = 775$ MeV), the pion mass ($m_\pi = 135$ MeV), and the pion decay constant ($f_\pi = 92.4$ MeV) to their experimental values. The vector meson masses are obtained by solving the EOM,

$$\partial_z \left(\frac{e^{-\Phi}}{z} \partial_z V_\rho(z) \right) + m_\rho^2 \frac{e^{-\Phi}}{z} V_\rho(z) = 0, \quad (17)$$

subject to the boundary conditions $V_\rho(0) = 0$ and $V_\rho'(\infty) = 0$. The decay constant of the ρ meson is given by

$$F_\rho = \frac{1}{g_5^2} \left. \frac{e^{-\Phi} \partial_z V_\rho(z)}{z} \right|_{z \rightarrow 0}, \quad (18)$$

where $V_\rho(z)$ denotes the normalized ground-state wave function satisfying $\int dz e^{-\Phi} V_\rho^2 / z = 1$.

To determine the pion mass, we derive the EOMs for the pseudoscalar sector from the bulk action. In the two-flavor improved soft-wall model, the equations take the form

$$\partial_z \left(\frac{e^{-\Phi}}{z} \partial_z \varphi \right) + g_5^2 \frac{\chi^2(z) e^{-\Phi}}{z^3} (\pi - \varphi) = 0, \quad (19)$$

$$q^2 \partial_z \varphi - g_5^2 \frac{\chi^2(z)}{z^2} \partial_z \pi = 0, \quad (20)$$

with boundary conditions $\varphi^a(0) = \partial_z \varphi^a(\infty) = \pi^a(0) = 0$. The pion mass is obtained by identifying $m_\pi^2 = q^2$. The pion wave function $\varphi(z)$ is normalized according to

$$\int_0^\infty dz \frac{e^{-\Phi}}{g_5^2} \left[\frac{(\partial_z \varphi)^2}{z} + \frac{g_5^2 \chi^2 (\pi - \varphi)^2}{z^3} \right] = 1. \quad (21)$$

For the 2 + 1-flavor soft-wall model, the above equations remain valid after replacing $\chi(z)$ by $\sqrt{2} \chi_u(z)$. Since the derivation of these equations has been discussed extensively in the literature, we do not repeat it here and refer the reader to Refs. [69, 70] for details. The pion decay constant is then computed from the normalized pion ground-state wave function as

$$f_\pi = \frac{1}{g_5^2} \left. \frac{e^{-\Phi} \partial_z \varphi(z)}{z} \right|_{z \rightarrow 0} = \frac{1}{g_5^2} \partial_z^2 \varphi(0). \quad (22)$$

To solve the above EOMs, we employ two independent numerical approaches implemented in *Mathematica*. The first is the conventional shooting method, which transforms the boundary-value problem into an initial-value problem. The second approach combines a spectral method with the `Eigensystem` routine and is found to be numerically more stable. We have verified that both methods yield consistent results. By fitting the ground-state ρ -meson mass, the pion mass, and the pion decay constant to their experimental values, the model parameters are determined as follows:

- SW1: $\mu_g = 473$ MeV, $\lambda_g = 1.7$, $\mu_c = 375$ MeV, $\sigma^{1/3} = 293$ MeV, $m_q = 3.3$ MeV;
- SW2: $\mu_g = 387.5$ MeV, $\lambda = 65.8$, $\mu_c = 1500$ MeV, $m_q = 3.18$ MeV;
- SW3: $\mu_g = 480$ MeV, $\lambda = 110$, $\mu_c = 1200$ MeV, $m_u = 3.25$ MeV, $m_s = 98$ MeV, and $\gamma = -25.25$.

Table I summarizes the ρ -meson and pion mass spectra obtained in the different models, where the values marked by an asterisk are taken as input. The corresponding pion decay constants are $f_\pi^{\text{SW1}} = 92.48$ MeV, $f_\pi^{\text{SW2}} = 92.47$ MeV, and $f_\pi^{\text{SW3}} = 92.35$ MeV. The results indicate that, except for the vector sector of the SW2 model—where the excited-state spectrum deviates from experimental data due to the constraint of fixing the ground-state mass—the improved soft-wall models exhibit overall good agreement with experimental observations. Table I also lists a subset of vector-meson decay constants at different excitation levels, which are used in the subsequent calculation of the vector current two-point correlation function. Nevertheless, the ground-state ρ -meson decay constants predicted by all three models are systematically lower than the experimental value, $F_\rho^{1/2} \simeq 348(1)$ MeV [72].

Model		0	1	2	3	4	5	6
Exp. [MeV]	m_ρ	775.26 ± 0.25	1465 ± 25	1720 ± 20	1909 ± 17	2150 ± 40	-	-
	m_π	135	1300 ± 100	1812 ± 12	2070 ± 35	2360 ± 25	-	-
SW1	m_ρ	775.5^*	1354	1667	1919	2140	2339	2523
	$F_\rho^{1/2}$	329.4	365.5	405	439.4	468.3	492.7	513.8
	m_π	135^*	1480	1828	2083	2300	2495	2674
SW2	m_ρ	775^*	1096	1342	1550	1733	1898	2050
	$F_\rho^{1/2}$	260	309.2	342.2	367.7	388.8	406.9	422.9
	m_π	135^*	1661	1900	2070	2220	2358	2487
SW3	m_ρ	775.1^*	1335	1714	1986	2201	2393	2572
	$F_\rho^{1/2}$	308	405.5	448.5	465	482.6	503.4	523
	m_π	135^*	1483	1858	2126	2332	2515	2687

TABLE I The ρ -meson and pion mass spectra, together with the corresponding ρ -meson decay constants F_ρ , calculated in units of MeV within different holographic QCD models, and compared with experimental values taken from the suggested quark-model assignments for observed light mesons [73].

IV. THE LO-HVP CONTRIBUTION OF a_μ

To set the stage, we introduce the HVP function, which plays a central role in the leading-order HVP (LO-HVP) contribution to the muon anomalous magnetic moment $(g - 2)_\mu$, following Refs. [74, 75]:

$$a_\mu^{\text{LO-HVP}} = 4\pi^2 \left(\frac{\alpha}{\pi}\right)^2 \int_0^\infty dQ^2 f(Q^2) \Pi_{\text{em}}^{\text{had}}(Q^2), \quad (23)$$

where $Q^2 = -q^2$ denotes the spacelike momentum squared, and

$$f(Q^2) = \frac{m_\mu^2 Q^2 Z^3 (1 - Q^2 Z)}{1 + m_\mu^2 Q^2 Z^2}, \quad Z = -\frac{Q^2 - \sqrt{Q^4 + 4m_\mu^2 Q^2}}{2m_\mu^2 Q^2}. \quad (24)$$

Here $\Pi_{\text{em}}^{\text{had}}(Q^2)$ denotes the hadronic component of the electromagnetic vacuum polarization function, defined through the two-point correlator of electromagnetic currents evaluated at spacelike momentum Q^2 , and renormalized such that $\Pi_{\text{em}}^{\text{had}}(0) = 0$. In holographic QCD, it can be extracted from the vector-current correlator; in the flavor-symmetric case,

$$\Pi_{\text{em}}^{\text{had}}(-q^2) = 2 \text{Tr}(Q_{\text{em}}^2) \Pi_V(-q^2), \quad (25)$$

where $Q_{\text{em}} = \text{diag}(\frac{2}{3}, -\frac{1}{3}, -\frac{1}{3}, \dots)$ is the quark charge matrix. Consequently, for the two-flavor and three-flavor cases, one obtains [76]

$$\Pi_{\text{em}(N_f=2)}^{\text{had}}(-q^2) = \frac{10}{9} \Pi_V(-q^2), \quad \Pi_{\text{em}(N_f=3)}^{\text{had}}(-q^2) = \frac{4}{3} \Pi_V(-q^2). \quad (26)$$

In this work, we restrict our analysis to the $N_f = 2$ case.

The vector current two-point function $\Pi_V(Q^2)$ is defined as

$$i \int d^4x e^{iqx} \langle 0 | T \{ J_V^{a\mu}(x) J_V^{b\nu}(0) \} | 0 \rangle = \delta^{ab} (q^2 \eta^{\mu\nu} - q^\mu q^\nu) \Pi_V(Q^2). \quad (27)$$

For the SW2 model, the vector current two-point function can be obtained from

$$\Pi_V(-q^2) = -\frac{e^{-\Phi}}{g_5^2} \frac{\partial_z V(q, z)}{q^2 z} \Big|_{z=\epsilon}, \quad (28)$$

where the limit $\epsilon \rightarrow 0$ is implied, and $V(q, z)$ denotes the vector bulk-to-boundary propagator, which is determined by solving the EOM for the transverse component of the gauge field,

$$\partial_z \left(\frac{e^{-\Phi}}{z} \partial_z V_\mu^a(q, z) \right) + \frac{q^2 e^{-\Phi}}{z} V_\mu^a(q, z) = 0, \quad (29)$$

subject to the boundary conditions $V(q, 0) = 1$ and $\partial_z V(q, \infty) = 0$. Since the vector sector of this model coincides with that of the original soft-wall model, an analytic solution for $V(q, z)$ can be obtained [77],

$$V(q, z) = \Gamma \left(1 - \frac{q^2}{4\mu_g^2} \right) U \left(-\frac{q^2}{4\mu_g^2}, 0, \mu_g^2 z^2 \right), \quad (30)$$

where Γ is the Gamma function and U denotes the Tricomi confluent hypergeometric function. Substituting this expression into Eq. (28), expanding in the small parameter ϵ , and performing the renormalization using $\psi(0) = -\gamma$, one obtains

$$\Pi_V^{\text{ren}}(Q^2) = \frac{1}{g_5^2} \left[\psi \left(\frac{Q^2}{4\mu_g^2} + 1 \right) + \gamma \right], \quad (31)$$

where $\psi(z) = \frac{d}{dz} \ln \Gamma(z)$ is the digamma function.

For the SW1 and SW3 models, the increased functional complexity prevents us from deriving a closed-form analytic expression. Therefore, following Refs. [72, 76], we evaluate the renormalized vector correlator, with the condition $\Pi_V^{\text{ren}}(0) = 0$, using

$$\Pi_V^{\text{ren}}(-q^2) = \sum_{n=1}^l \frac{q^2 F_{\rho^n}^2}{(q^2 - m_{\rho^n}^2) m_{\rho^n}^4} + \mathcal{O} \left(\frac{q^2}{m_{\rho^{l+1}}^2} \right), \quad (32)$$

where m_{ρ^n} denotes the mass of the n -th vector meson and $F_{\rho^n}^{1/2}$ its corresponding decay constant. Provided that l is taken sufficiently large so that enough resonances are included in the summation, this expression accurately reproduces the vector correlator.

Substituting the vector-current correlator into Eq. (23), we compute the LO-HVP contribution to the muon anomalous magnetic moment for $N_f = 2$ within the various improved

Model	SW1	SW2	SW3	HW	SW	TC (fit 1 2)
$a_{\mu(N_f=2)}^{\text{LO-HVP}} \times 10^{-10}$	482.5	276.4	404.0	476.9	276.4	442.3 403.6

TABLE II The LO-HVP contribution to a_{μ} for $N_f = 2$ obtained from different holographic QCD models. The results for the hard-wall (HW), original soft-wall (SW), and tachyon condensation (TC) models are taken from Ref. [72].

soft-wall models; the results are summarized in Table II. For comparison, we also quote the corresponding results obtained in the hard-wall model [38, 40], the original soft-wall model [39, 78], and the tachyon condensation model [79–81]. In addition, we evaluate the integrand of Eq. (23) as a function of Q^2 , as shown in Fig. 1. The SW1 model yields the largest result, slightly exceeding that of the hard-wall model, while the SW3 prediction lies in an intermediate range and nearly overlaps with the result of the TC model (fit 2). Among the models considered, SW2 produces the smallest value and thus gives the lowest LO-HVP contribution.

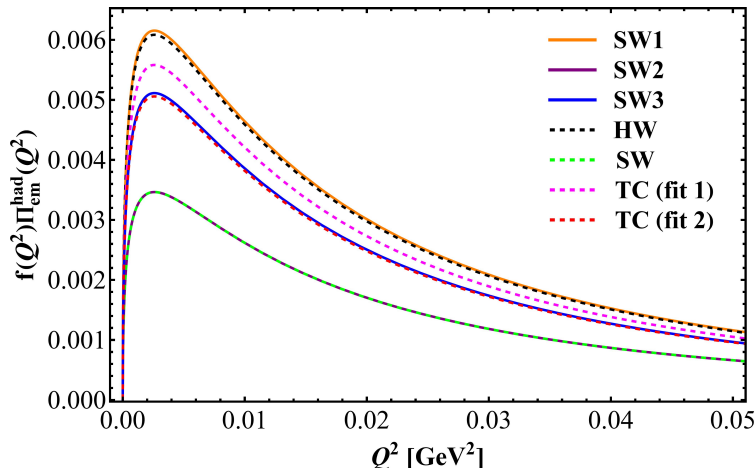


FIG.1. The integrand $f(Q^2)\Pi_{\text{em}}^{\text{had}}(Q^2)$ as a function of Q^2 computed in different models: SW1 (orange solid line), SW2 (purple solid line), SW3 (blue solid line), the hard-wall model (black dashed line), the original soft-wall model (green dashed line), and the tachyon condensation model (magenta and red dashed lines).

From Table II, it is evident that while the SW2 results coincide with those of the original soft-wall model, the other improved soft-wall constructions yield larger values; in particular, the SW1 model provides the largest $N_f = 2$ LO-HVP contribution. By incorporating infrared modifications that more faithfully capture essential dynamical features of QCD, the improved soft-wall models not only reproduce a ρ -meson mass spectrum in good agreement with experimental data but also predict a ground-state ρ -meson decay constant much closer to the experimental value than that obtained in the original soft-wall model. Given the strong sensitivity of the pseudoscalar sector to infrared dynamics, this improved description of the mass spectrum and decay constants naturally feeds back into the pseudoscalar channel, leading to enhanced numerical predictions for the LO-HVP contribution.

It has been argued that the two-flavor holographic QCD predictions are most appropriately compared with the contributions from the two- and three-pion states as well as the

$\pi^0\gamma$ intermediate state [72]. The corresponding dispersive determinations yield $(558 \pm 4) \times 10^{-10}$ [82] and $(555 \pm 3) \times 10^{-10}$ [83], while resonance chiral theory gives $(559.18 \pm 2.75) \times 10^{-10}$ [14, 15]. We find that all holographic QCD models exhibit sizable deviations from the dispersive and resonance chiral theory results for the LO-HVP contribution. Even in the most favorable case, the holographic prediction reaches only about 87% of the dispersive value. This discrepancy may be attributed to the fact that the vector-meson decay constants predicted by these models remain systematically lower than their experimental counterparts [72]. We modify the parameters of the SW1 model by choosing $\lambda_g = 1.8$ and $\mu_g = 503.5$ MeV, which yield $m_\rho = 775.2$ MeV and $F_\rho^{1/2} = 347.2$ MeV, both consistent with the experimental values. Recalculating the LO-HVP contribution with these adjusted parameters, we obtain $a_\mu^{\text{LO-HVP}} = 573.5 \times 10^{-10}$, which is slightly higher than the corresponding dispersive and resonance chiral theory estimates.

V. HADRONIC LIGHT-BY-LIGHT CONTRIBUTION

A. Pion transition form factor

To evaluate the pseudoscalar-meson contribution to the HLbL scattering part of the muon anomalous magnetic moment, we first consider the transition form factor (TFF) of the neutral pion into two photons, defined by

$$i \int d^4x e^{iqx} \langle 0 | T \{ j_\mu(x) j_\nu(0) \} | \pi^0(p) \rangle = \epsilon_{\mu\nu\rho\sigma} q^\rho p^\sigma F_{\pi^0\gamma^*\gamma^*}(q^2, (p-q)^2), \quad (33)$$

where $j_\mu(x)$ denotes the hadronic electromagnetic current. The holographic computation of $F_{\pi^0\gamma^*\gamma^*}$ leads to the standard expression [84–88],

$$F(Q_1^2, Q_2^2) = -\frac{N_c}{12\pi^2} K(Q_1^2, Q_2^2), \quad (34)$$

where $K(Q_1^2, Q_2^2)$ is obtained by integrating the product of the two photon bulk-to-boundary propagators and the holographic pion wave function along the fifth dimension, as dictated by the Chern–Simons action:

$$K(Q_1^2, Q_2^2) = -\int_0^\infty V(Q_1, z) V(Q_2, z) \partial_z \varphi(z) dz. \quad (35)$$

Here, $V(q, z)$ is determined by solving Eq. (29), and $\varphi(z)$ denotes the normalized pion wave function according to Eq. (21). Fig. 2 shows the normalized ground-state wave functions of π^0 calculated from different models. It can be observed that the values of wave functions exhibit certain discrepancies at small radial coordinate z , whereas as z increases, they gradually approach the constant value $1/f_\pi$ in the chiral limit.

For the evaluation of $F(Q_1^2, Q_2^2)$, we follow the convention of Ref. [89], noting that the expression given in Ref. [59] differs slightly. This discrepancy originates from different normalization conventions for the pion wave function. If we adopt the following normalization condition for the SW1 and SW2 models¹:

$$\int_0^\infty dz \frac{e^{-\Phi}}{g_5^2 f_\pi^2} \left(\frac{(\partial_z \varphi)^2}{z} + \frac{g_5^2 \chi^2 (\pi - \varphi)^2}{z^3} \right) = 1, \quad (36)$$

¹ For the SW3 case, one simply replaces χ with $\sqrt{2}\chi_u$.

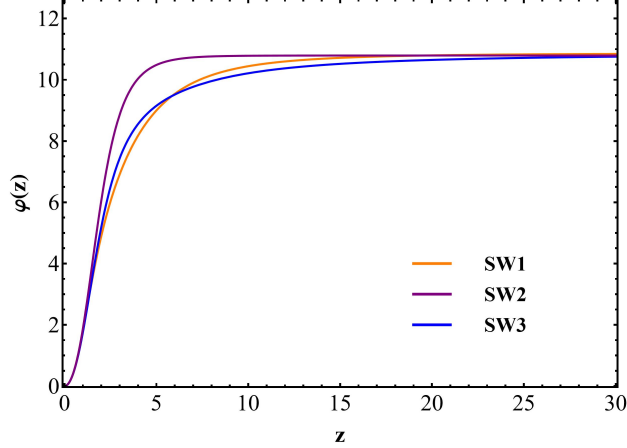


FIG.2. Normalized ground-state wave functions $\varphi(z)$ of π_0 in different holographic models.

the wave function approaches unity at large z . With this normalization, one may equivalently follow the procedure of Ref. [59] to compute $F(Q_1^2, Q_2^2)$.

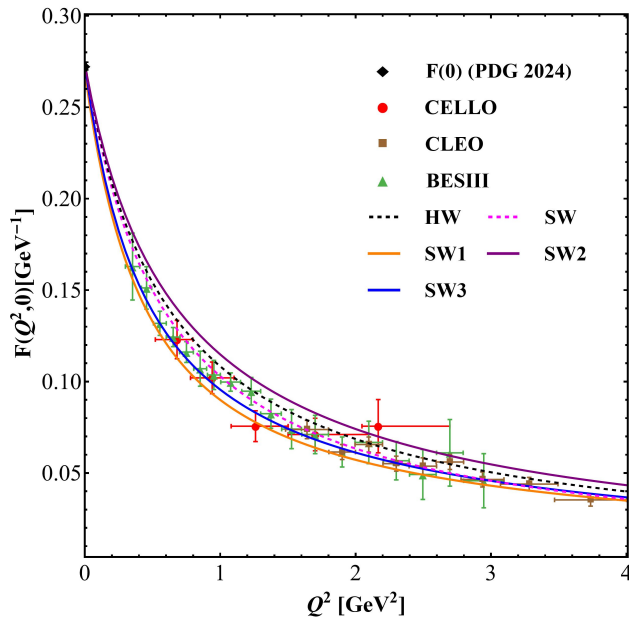


FIG.3. Comparison of the Q^2 dependence of $F(Q^2, 0)$ computed in various holographic models with experimental data from CELLO, CLEO, and BESIII [24].

In Fig. 3, we compare the spacelike π^0 TFF obtained from various holographic models with the experimental data compiled in Ref. [24], focusing on the momentum range $0 \leq Q^2 \leq 4 \text{ GeV}^2$; for reference, we also display the results from the hard-wall model and the original soft-wall model, where both models are implemented following the setup adopted in Ref. [59]. At $Q^2 = 0$, the three models give $F(0, 0) = 0.2746 \text{ GeV}^{-1}$ for SW1, $F(0, 0) = 0.2733 \text{ GeV}^{-1}$ for SW2, and $F(0, 0) = 0.2735 \text{ GeV}^{-1}$ for SW3. In the Q^2 range displayed in the figure, all three improved soft-wall models show good agreement with the experimental data, with the SW2 curve lying slightly above that of the hard-wall model, whereas the SW1 and SW3 results are somewhat lower. Fig. 4 shows the Q^2 dependence

of the singly-virtual TFF computed in different holographic models over a broad kinematic range. As can be seen, the form factors obtained from the three improved soft-wall models are consistent with the available experimental data. At large Q^2 , the asymptotic Brodsky–Lepage behavior is correctly reproduced, with the quantity $Q^2 F(Q^2, 0)$ approaching the limit $2f_\pi$ [90]. Furthermore, no significant rise is observed for $Q^2 > 10 \text{ GeV}^2$, in contrast to the trend reported by the BaBar Collaboration.

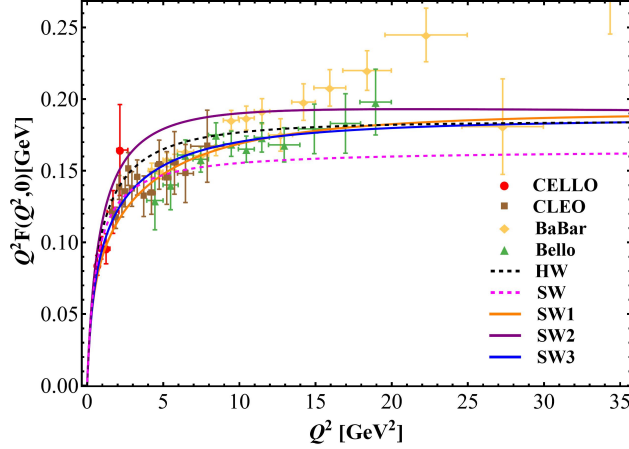


FIG.4. The singly-virtual form factor $Q^2 F(Q^2, 0)$ calculated in the holographic models, compared with the experimental data [91–94].

In the momentum-symmetric case $Q_1^2 = Q_2^2$, the diagonal π^0 TFF computed from different holographic models are shown in Fig. 5, together with the results and uncertainties obtained from the dispersive approach. The SW1 and SW3 models lie closest to the dispersive determination and remain slightly below the prediction of the hard-wall model, whereas the SW2 model yields comparatively larger values than both the other holographic models and the dispersive result.

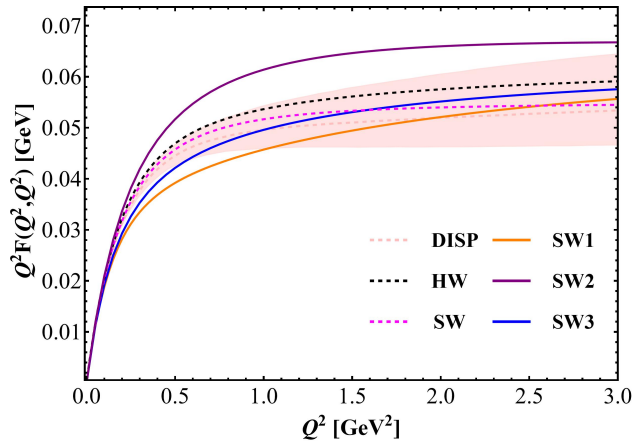


FIG.5. The Q^2 dependence of the diagonal form factor $Q^2 F(Q^2, Q^2)$ in the low- Q^2 region, where the light-red error band denotes the result obtained from the dispersive approach [23].

Furthermore, Fig. 6 presents the three-dimensional representation of π_0 TFF obtained through different models in the case of large momentum Q . A prominent feature of the holo-

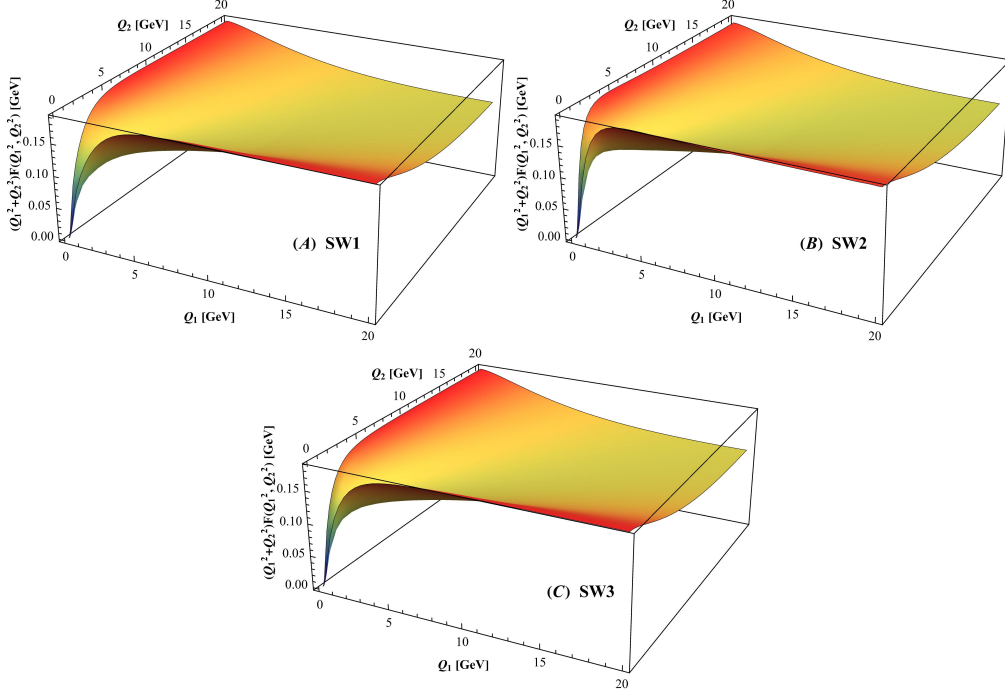


FIG.6. Three-dimensional representation of $(Q_1^2 + Q_2^2)F(Q_1^2, Q_2^2)$ at large momentum Q in different models.

graphic QCD framework is its capacity to extend the calculation into the deep Euclidean region ($Q^2 \gg \Lambda_{\text{QCD}}^2$) with high numerical stability. Unlike some phenomenological models that rely on truncated expansions or limited momentum parameterizations, the holographic approach naturally incorporates the correct high-energy scaling. This capability allows for a more reliable determination of the TFF over an exceptionally broad range of Q . Consequently, by reducing the reliance on arbitrary extrapolations at high momenta, the holographic model significantly suppresses the systematic uncertainties in the subsequent calculation of the HLbL scattering contribution to the muon $g - 2$.

B. Numerical results

By computing the $\pi^0 \rightarrow \gamma^* \gamma^*$ transition form factor within the holographic framework and inserting the result into the standard expression for the pseudoscalar-exchange contribution, we are able to evaluate the pole contribution to a_μ^{HLbL} in our holographic QCD models. According to Ref. [95], the expression takes the form

$$\begin{aligned}
 a_\mu^{\text{HLbL}} = & \left(\frac{\alpha}{\pi}\right)^3 \int_0^\infty dQ_1 \int_0^\infty dQ_2 \int_{-1}^1 d\tau \left(w_1(Q_1, Q_2, \tau) F(Q_1^2, (Q_1 + Q_2)^2) F(Q_2^2, 0) \right. \\
 & \left. + w_2(Q_1, Q_2, \tau) F(Q_1^2, Q_2^2) F((Q_1 + Q_2)^2, 0) \right), \quad (37)
 \end{aligned}$$

where the weight functions w_1 and w_2 are given in Appendix A of Ref. [95]. The integral is evaluated numerically in *Mathematica* using the `LocalAdaptive` integration method, with integration ranges chosen as $Q \in [0, 20 \text{ GeV}]$ and the holographic coordinate $z \in [10^{-6} \text{ GeV}^{-1}, 30 \text{ GeV}^{-1}]$. Although the integral is already well saturated for $Q > 5 \text{ GeV}$,

we extend the upper limit to 20 GeV to ensure numerical stability. The resulting π^0 -pole contributions to a_μ^{HLbL} obtained from different holographic models are summarized in Table III. Furthermore, following the procedure of Ref. [59], we perform a simple extrapolation to estimate the η and η' contributions to a_μ by employing the same function $K(Q_1^2, Q_2^2)$ obtained in the chiral limit for all holographic models. In this extrapolation, the normalization constant $F(0, 0)$ is rescaled to match the central experimental values [24], namely $F_\eta(0, 0)/F_{\pi^0}(0, 0) = 0.2736/0.2725$ and $F_{\eta'}(0, 0)/F_{\pi^0}(0, 0) = 0.3412/0.2725$, while the physical masses of the η and η' are used in the numerical evaluation.

$a_\mu^{\text{HLbL}} \times 10^{-11}$	SW1	SW2	SW3	HW	SW	WP(2025) [8]	LQCD [96]
$a_\mu^{\pi^0}$	56.1	68.6	58.7	65.2	63.1	$63.6^{+3.0}_{-2.5}$	$57.8 \pm 1.8 \pm 0.9$
a_μ^η	15.1	19.8	15.9	18.2	17.3	14.72 ± 0.87	$11.6 \pm 1.6 \pm 0.5 \pm 1.1$
$a_\mu^{\eta'}$	10.8	14.5	11.4	13.2	12.4	13.56 ± 0.70	$15.7 \pm 3.9 \pm 1.1 \pm 1.3$

TABLE III The pole contributions of π^0 , η , and η' to a_μ^{HLbL} . The η and η' contributions are obtained using the same extrapolation procedure as in Ref. [59]. “WP” denotes the white paper result [8], and “LQCD” refers to lattice QCD data from the BMW Collaboration [96].

From Table III, we observe that the SW1 and SW3 models yield very similar predictions for $a_\mu^{\pi^0}$, both of which are smaller than the results obtained in the hard-wall and original soft-wall models, whereas the SW2 model gives a noticeably larger value. For comparison, Table III also includes the latest determinations reported in the White Paper and by the BMW lattice QCD collaboration. Additional lattice calculations by the Mainz group give $a_\mu^{\pi^0\text{-pole}} = 59.7(3.6) \times 10^{-11}$ [97], while dispersive analyses yield $a_\mu^{\pi^0\text{-pole}} = 63.0^{+2.7}_{-2.1} \times 10^{-11}$ [23, 98] and the Canterbury approximant method gives $a_\mu^{\pi^0\text{-pole}} = 63.6(2.7) \times 10^{-11}$ [99]. More recently, resonance chiral theory has reported $a_\mu^{\pi^0\text{-pole}} \approx 61.6(1.8) \times 10^{-11}$ [28]. These independent determinations are mutually consistent within uncertainties, indicating that the pion-pole contribution to the HLbL correction is now relatively well constrained.

Although the three improved holographic models yield similar meson spectra consistent with experimental data, their underlying constructions differ in the infrared implementation. In particular, the SW1 and SW3 models modify the dilaton profile, leading to a more refined and mutually consistent description of the hadron spectrum, whereas the SW2 model retains the original soft-wall dilaton structure and thus remains closer to the baseline setup. These structural differences translate into non-negligible variations in the pion transition form factor, especially in the low- and intermediate-momentum regions that dominate the HLbL loop integral. Consequently, the SW1 and SW3 predictions for the pseudoscalar-pole contribution lie below the value quoted in the White Paper and are close to lattice QCD determinations from the BMW collaboration and the Mainz group, while the SW2 prediction is higher than the White Paper and other data-driven estimates. This pattern indicates that, in holographic soft-wall constructions, achieving an accurate description of the hadron mass spectrum, particularly through a suitable infrared modification, plays a crucial role in obtaining reliable predictions for more sensitive observables such as the HLbL contribution.

It is worth noting that the present work primarily includes contributions from ground-state pseudoscalar mesons. Given that holographic models predict an infinite tower of excited states, systematically incorporating and summing these contributions is of considerable importance. However, recent studies [100] have shown that a broad class of soft-wall models suffers from divergences associated with excited-state contributions in both the pseudoscalar and axial-vector channels. Although modifications of the Chern–Simons term have been proposed to mitigate this issue, it was also noted in Ref. [100] that the resulting transition form factors exhibit significant deviations from experimental data. This points to a nontrivial tension between curing the divergence of excited-state contributions and maintaining consistency with experimental form factors, and calls for further investigation in future studies.

Overall, these findings highlight an important lesson for future holographic model building: achieving realistic predictions for the HLbL contribution requires not only an accurate description of infrared observables, such as resonance spectra and decay constants, but also the proper implementation of the short-distance constraints dictated by QCD. The pseudoscalar TFF thus serves as a particularly stringent discriminator among different holographic constructions and provides a key benchmark for further model improvements.

VI. SUMMARY AND DISCUSSION

In this work, we have carried out a systematic investigation of the hadronic contributions to the muon anomalous magnetic moment within three infrared-improved soft-wall AdS/QCD models, denoted as SW1, SW2, and SW3. These models are constructed to provide a more realistic description of low-energy hadronic observables—particularly meson mass spectra and decay constants—than the original hard-wall and soft-wall frameworks. Within a unified holographic setup, we have evaluated both the leading-order HVP contribution and the pseudoscalar-pole contribution to HLbL scattering.

For the LO-HVP contribution, the improved soft-wall models generally yield values that remain somewhat below data-driven dispersive determinations. Our analysis shows that this discrepancy is closely correlated with the imperfect reproduction of the ρ -meson decay constant, to which the HVP contribution is particularly sensitive. Once the vector decay constant is adjusted to its experimental value, the holographic prediction for the LO-HVP contribution becomes consistent with the dispersive estimate, indicating that the main source of deviation is tied to the vector sector of the models.

In contrast, the pseudoscalar-pole contribution to HLbL scattering exhibits a more pronounced model dependence. Although all three models provide a reasonable description of the pseudoscalar transition form factor and remain broadly consistent with available experimental data, noticeable differences appear in the intermediate momentum region that dominates the HLbL integral. Consequently, the predicted HLbL contributions display a non-negligible spread among these three models, which provides a useful estimate of the intrinsic model uncertainty associated with holographic descriptions of the pseudoscalar transition form factor. It should be emphasized that only the pseudoscalar pole contribution to the HLbL scattering is considered in this study. A complete evaluation requires the inclusion of additional intermediate states, which we leave for future work.

Taken together, our results indicate that infrared-improved soft-wall models represent a meaningful step beyond the classic holographic constructions in the study of hadronic contributions to the muon anomalous magnetic moment. While the large- N_c nature of the holographic approach and the absence of explicit quark-mass effects limit the precision

achievable compared with state-of-the-art lattice QCD or dispersive analyses, these models nonetheless offer a valuable complementary perspective. In particular, holographic models provide analytic control over resonance dynamics and naturally incorporate an infinite tower of hadronic states, allowing one to explore the sensitivity of a_μ to different realizations of low-energy QCD dynamics in a controlled manner.

From a broader perspective, our analysis shows that improved holographic QCD models can serve as an intermediate framework bridging purely data-driven approaches and first-principles lattice calculations. Systematic comparisons with dispersive reconstructions and independent lattice determinations will be essential for assessing the reliability and limitations of holographic predictions. Future extensions of this work may include refined treatments of chiral symmetry breaking, explicit quark-mass effects, and additional hadronic channels, with the aim of reducing model dependence and further improving the phenomenological relevance of holographic approaches to the muon $g - 2$.

ACKNOWLEDGMENTS

The authors are grateful to Xin-Yi Liu for the technical assistance regarding numerical algorithms, and to Yi-Hao Zhang for valuable discussions. This work is supported by Hunan Provincial Natural Science Foundation of China (Grants No. 2023JJ30115 and No. 2024JJ3004). L.-Y. Dai thanks the support from National Natural Science Foundation of China (NSFC) with Grants No.12322502, 12335002.

-
- [1] J. S. Schwinger, On Quantum electrodynamics and the magnetic moment of the electron, [Phys. Rev. **73**, 416 \(1948\)](#).
 - [2] J. Bailey *et al.* (CERN-Mainz-Daresbury), Final Report on the CERN Muon Storage Ring Including the Anomalous Magnetic Moment and the Electric Dipole Moment of the Muon, and a Direct Test of Relativistic Time Dilation, [Nucl. Phys. B **150**, 1 \(1979\)](#).
 - [3] G. W. Bennett *et al.* (Muon $g-2$), Final Report of the Muon E821 Anomalous Magnetic Moment Measurement at BNL, [Phys. Rev. D **73**, 072003 \(2006\)](#), [arXiv:hep-ex/0602035](#).
 - [4] B. Abi *et al.* (Muon $g-2$), Measurement of the Positive Muon Anomalous Magnetic Moment to 0.46 ppm, [Phys. Rev. Lett. **126**, 141801 \(2021\)](#), [arXiv:2104.03281 \[hep-ex\]](#).
 - [5] D. P. Aguillard *et al.* (Muon $g-2$), Measurement of the Positive Muon Anomalous Magnetic Moment to 0.20 ppm, [Phys. Rev. Lett. **131**, 161802 \(2023\)](#), [arXiv:2308.06230 \[hep-ex\]](#).
 - [6] D. P. Aguillard *et al.* (Muon $g-2$), Measurement of the Positive Muon Anomalous Magnetic Moment to 127 ppb, [Phys. Rev. Lett. **135**, 101802 \(2025\)](#), [arXiv:2506.03069 \[hep-ex\]](#).
 - [7] T. Aoyama *et al.*, The anomalous magnetic moment of the muon in the Standard Model, [Phys. Rept. **887**, 1 \(2020\)](#), [arXiv:2006.04822 \[hep-ph\]](#).
 - [8] R. Aliberti *et al.*, The anomalous magnetic moment of the muon in the Standard Model: an update, [Phys. Rept. **1143**, 1 \(2025\)](#), [arXiv:2505.21476 \[hep-ph\]](#).
 - [9] M. Davier, A. Hoecker, B. Malaescu, and Z. Zhang, Reevaluation of the hadronic vacuum polarisation contributions to the Standard Model predictions of the muon $g - 2$ and $\alpha(m_Z^2)$ using newest hadronic cross-section data, [Eur. Phys. J. C **77**, 827 \(2017\)](#), [arXiv:1706.09436 \[hep-ph\]](#).

- [10] B.-L. Hoid, M. Hoferichter, and B. Kubis, Hadronic vacuum polarization and vector-meson resonance parameters from $e^+e^- \rightarrow \pi^0\gamma$, *Eur. Phys. J. C* **80**, 988 (2020), [arXiv:2007.12696 \[hep-ph\]](#).
- [11] M. Hoferichter and T. Teubner, Mixed Leptonic and Hadronic Corrections to the Anomalous Magnetic Moment of the Muon, *Phys. Rev. Lett.* **128**, 112002 (2022), [arXiv:2112.06929 \[hep-ph\]](#).
- [12] M. Benayoun, L. DelBuono, and F. Jegerlehner, BHLS₂ upgrade: τ spectra, muon HVP and the $[\pi^0, \eta, \eta']$ system, *Eur. Phys. J. C* **82**, 184 (2022), [arXiv:2105.13018 \[hep-ph\]](#).
- [13] J.-Y. Yi, Z.-Y. Wang, and C. W. Xiao, Study of the pion vector form factor and its contribution to the muon $g - 2$, *Phys. Rev. D* **104**, 116017 (2021), [arXiv:2107.09535 \[hep-ph\]](#).
- [14] W. Qin, L.-Y. Dai, and J. Portoles, Two and three pseudoscalar production in e^+e^- annihilation and their contributions to $(g - 2)_\mu$, *JHEP* **03**, 092, [arXiv:2011.09618 \[hep-ph\]](#).
- [15] S.-J. Wang, Z. Fang, and L.-Y. Dai, Two body final states production in electron-positron annihilation and their contributions to $(g - 2)_\mu$, *JHEP* **07**, 037, [arXiv:2302.08859 \[hep-ph\]](#).
- [16] B.-H. Qin, W. Qin, and L.-Y. Dai, Study of electron-positron annihilation into $K\bar{K}\pi$ within resonance chiral theory, *Phys. Rev. D* **111**, 034025 (2025), [arXiv:2403.14294 \[hep-ph\]](#).
- [17] M. Hayakawa and T. Kinoshita, Pseudoscalar pole terms in the hadronic light by light scattering contribution to muon $g - 2$, *Phys. Rev. D* **57**, 465 (1998), [Erratum: *Phys.Rev.D* 66, 019902 (2002)], [arXiv:hep-ph/9708227](#).
- [18] A. Guevara, P. Roig, and J. J. Sanz-Cillero, Pseudoscalar pole light-by-light contributions to the muon $(g - 2)$ in Resonance Chiral Theory, *JHEP* **06**, 160, [arXiv:1803.08099 \[hep-ph\]](#).
- [19] K. Raya, A. Bashir, and P. Roig, Contribution of neutral pseudoscalar mesons to a_μ^{HLbL} within a Schwinger-Dyson equations approach to QCD, *Phys. Rev. D* **101**, 074021 (2020), [arXiv:1910.05960 \[hep-ph\]](#).
- [20] E. J. Estrada, S. González-Solís, A. Guevara, and P. Roig, Improved π^0, η, η' transition form factors in resonance chiral theory and their a_μ^{HLbL} contribution, *JHEP* **12**, 203, [arXiv:2409.10503 \[hep-ph\]](#).
- [21] E. J. Estrada and P. Roig, Tensor meson pole contributions to the HLbL piece of a_μ^{HLbL} within R χ T, *JHEP* **01**, 070, [arXiv:2504.00448 \[hep-ph\]](#).
- [22] G. Colangelo, M. Hoferichter, M. Procura, and P. Stoffer, Dispersive approach to hadronic light-by-light scattering, *JHEP* **09**, 091, [arXiv:1402.7081 \[hep-ph\]](#).
- [23] M. Hoferichter, B.-L. Hoid, B. Kubis, S. Leupold, and S. P. Schneider, Dispersion relation for hadronic light-by-light scattering: pion pole, *JHEP* **10**, 141, [arXiv:1808.04823 \[hep-ph\]](#).
- [24] I. Danilkin, C. F. Redmer, and M. Vanderhaeghen, The hadronic light-by-light contribution to the muon's anomalous magnetic moment, *Prog. Part. Nucl. Phys.* **107**, 20 (2019), [arXiv:1901.10346 \[hep-ph\]](#).
- [25] C. Alexandrou *et al.* (Extended Twisted Mass), $\eta \rightarrow \gamma^*\gamma^*$ transition form factor and the hadronic light-by-light η -pole contribution to the muon $g - 2$ from lattice QCD, *Phys. Rev. D* **108**, 054509 (2023), [arXiv:2212.06704 \[hep-lat\]](#).
- [26] C. Alexandrou *et al.* (Extended Twisted Mass), Pion transition form factor from twisted-mass lattice QCD and the hadronic light-by-light π^0 -pole contribution to the muon $g - 2$, *Phys. Rev. D* **108**, 094514 (2023), [arXiv:2308.12458 \[hep-lat\]](#).
- [27] S. Holz, M. Hoferichter, B.-L. Hoid, and B. Kubis, Precision Evaluation of the η - and η' -Pole Contributions to Hadronic Light-by-Light Scattering in the Anomalous Magnetic Moment of the Muon, *Phys. Rev. Lett.* **134**, 171902 (2025), [arXiv:2411.08098 \[hep-ph\]](#).

- [28] Y.-H. Zhang, S.-Z. Jiang, and L.-Y. Dai, Study of transition form factors of the lightest pseudoscalars, (2025), [arXiv:2509.06471 \[hep-ph\]](#).
- [29] F. Jegerlehner, *The Anomalous Magnetic Moment of the Muon*, Vol. 274 (Springer, Cham, 2017).
- [30] F. V. Ignatov *et al.* (CMD-3), Measurement of the $e^+e^- \rightarrow \pi^+\pi^-$ cross section from threshold to 1.2 GeV with the CMD-3 detector, *Phys. Rev. D* **109**, 112002 (2024), [arXiv:2302.08834 \[hep-ex\]](#).
- [31] T. Blum, N. Christ, M. Hayakawa, T. Izubuchi, L. Jin, C. Jung, and C. Lehner, Hadronic Light-by-Light Scattering Contribution to the Muon Anomalous Magnetic Moment from Lattice QCD, *Phys. Rev. Lett.* **124**, 132002 (2020), [arXiv:1911.08123 \[hep-lat\]](#).
- [32] G. Colangelo, M. Hoferichter, B. Kubis, M. Procura, and P. Stoffer, Towards a data-driven analysis of hadronic light-by-light scattering, *Phys. Lett. B* **738**, 6 (2014), [arXiv:1408.2517 \[hep-ph\]](#).
- [33] S. Borsanyi *et al.*, Leading hadronic contribution to the muon magnetic moment from lattice QCD, *Nature* **593**, 51 (2021), [arXiv:2002.12347 \[hep-lat\]](#).
- [34] T. Blum *et al.* (RBC, UKQCD), Update of Euclidean windows of the hadronic vacuum polarization, *Phys. Rev. D* **108**, 054507 (2023), [arXiv:2301.08696 \[hep-lat\]](#).
- [35] E. Witten, Anti de Sitter space and holography, *Adv. Theor. Math. Phys.* **2**, 253 (1998), [arXiv:hep-th/9802150](#).
- [36] S. S. Gubser, I. R. Klebanov, and A. M. Polyakov, Gauge theory correlators from noncritical string theory, *Phys. Lett. B* **428**, 105 (1998), [arXiv:hep-th/9802109](#).
- [37] J. M. Maldacena, The Large N limit of superconformal field theories and supergravity, *Adv. Theor. Math. Phys.* **2**, 231 (1998), [arXiv:hep-th/9711200](#).
- [38] J. Erlich, E. Katz, D. T. Son, and M. A. Stephanov, QCD and a holographic model of hadrons, *Phys. Rev. Lett.* **95**, 261602 (2005), [arXiv:hep-ph/0501128](#).
- [39] A. Karch, E. Katz, D. T. Son, and M. A. Stephanov, Linear confinement and AdS/QCD, *Phys. Rev. D* **74**, 015005 (2006), [arXiv:hep-ph/0602229](#).
- [40] L. Da Rold and A. Pomarol, Chiral symmetry breaking from five dimensional spaces, *Nucl. Phys. B* **721**, 79 (2005), [arXiv:hep-ph/0501218](#).
- [41] M. Jarvinen and E. Kiritsis, Holographic Models for QCD in the Veneziano Limit, *JHEP* **03**, 002, [arXiv:1112.1261 \[hep-ph\]](#).
- [42] D. Arean, I. Iatrakis, M. Järvinen, and E. Kiritsis, V-QCD: Spectra, the dilaton and the S-parameter, *Phys. Lett. B* **720**, 219 (2013), [arXiv:1211.6125 \[hep-ph\]](#).
- [43] D. Li and M. Huang, Dynamical holographic QCD model for glueball and light meson spectra, *JHEP* **11**, 088, [arXiv:1303.6929 \[hep-ph\]](#).
- [44] E. Folco Capossoli, M. A. Martín Contreras, D. Li, A. Vega, and H. Boschi-Filho, Hadronic spectra from deformed AdS backgrounds, *Chin. Phys. C* **44**, 064104 (2020), [arXiv:1903.06269 \[hep-ph\]](#).
- [45] D. Li and M. Huang, Chiral phase transition of QCD with $N_f = 2+1$ flavors from holography, *JHEP* **02**, 042, [arXiv:1610.09814 \[hep-ph\]](#).
- [46] X. Chen, L. Zhang, D. Li, D. Hou, and M. Huang, Gluodynamics and deconfinement phase transition under rotation from holography, *JHEP* **07**, 132, [arXiv:2010.14478 \[hep-ph\]](#).
- [47] D. Li, M. Huang, and Q.-S. Yan, A dynamical soft-wall holographic QCD model for chiral symmetry breaking and linear confinement, *Eur. Phys. J. C* **73**, 2615 (2013), [arXiv:1206.2824 \[hep-th\]](#).

- [48] X. Chen and M. Huang, Machine learning holographic black hole from lattice QCD equation of state, *Phys. Rev. D* **109**, L051902 (2024), [arXiv:2401.06417 \[hep-ph\]](#).
- [49] S. He, S.-Y. Wu, Y. Yang, and P.-H. Yuan, Phase Structure in a Dynamical Soft-Wall Holographic QCD Model, *JHEP* **04**, 093, [arXiv:1301.0385 \[hep-th\]](#).
- [50] Z. Fang, S. He, and D. Li, Chiral and Deconfining Phase Transitions from Holographic QCD Study, *Nucl. Phys. B* **907**, 187 (2016), [arXiv:1512.04062 \[hep-ph\]](#).
- [51] G. F. de Teramond and S. J. Brodsky, Hadronic spectrum of a holographic dual of QCD, *Phys. Rev. Lett.* **94**, 201601 (2005), [arXiv:hep-th/0501022](#).
- [52] Y.-Q. Sui, Y.-L. Wu, Z.-F. Xie, and Y.-B. Yang, Prediction for the Mass Spectra of Resonance Mesons in the Soft-Wall AdS/QCD with a Modified 5D Metric, *Phys. Rev. D* **81**, 014024 (2010), [arXiv:0909.3887 \[hep-ph\]](#).
- [53] T. Gherghetta, J. I. Kapusta, and T. M. Kelley, Chiral symmetry breaking in the soft-wall AdS/QCD model, *Phys. Rev. D* **79**, 076003 (2009), [arXiv:0902.1998 \[hep-ph\]](#).
- [54] K. Chelabi, Z. Fang, M. Huang, D. Li, and Y.-L. Wu, Chiral Phase Transition in the Soft-Wall Model of AdS/QCD, *JHEP* **04**, 036, [arXiv:1512.06493 \[hep-ph\]](#).
- [55] H. Boschi-Filho, N. R. F. Braga, and H. L. Carrion, Glueball Regge trajectories from gauge/string duality and the Pomeron, *Phys. Rev. D* **73**, 047901 (2006), [arXiv:hep-th/0507063](#).
- [56] J.-Y. Shen, X.-Y. Liu, J.-R. Wu, Y.-L. Wu, and Z. Fang, Toward a holographic realization of the 2+1-flavor QCD phase structure, *Phys. Rev. D* **112**, L111504 (2025), [arXiv:2511.11273 \[hep-ph\]](#).
- [57] X.-Y. Liu, Y.-L. Wu, and Z. Fang, Axial-anomaly effects and chiral phase structure in holographic QCD, (2026), [arXiv:2603.12616 \[hep-ph\]](#).
- [58] L. Cappiello, O. Cata, and G. D'Ambrosio, The hadronic light by light contribution to the $(g - 2)_\mu$ with holographic models of QCD, *Phys. Rev. D* **83**, 093006 (2011), [arXiv:1009.1161 \[hep-ph\]](#).
- [59] J. Leutgeb, J. Mager, and A. Rebhan, Pseudoscalar transition form factors and the hadronic light-by-light contribution to the anomalous magnetic moment of the muon from holographic QCD, *Phys. Rev. D* **100**, 094038 (2019), [Erratum: *Phys.Rev.D* 104, 059903 (2021)], [arXiv:1906.11795 \[hep-ph\]](#).
- [60] J. Leutgeb and A. Rebhan, Axial vector transition form factors in holographic QCD and their contribution to the anomalous magnetic moment of the muon, *Phys. Rev. D* **101**, 114015 (2020), [arXiv:1912.01596 \[hep-ph\]](#).
- [61] J. Leutgeb and A. Rebhan, Hadronic light-by-light contribution to the muon $g - 2$ from holographic QCD with massive pions, *Phys. Rev. D* **104**, 094017 (2021), [arXiv:2108.12345 \[hep-ph\]](#).
- [62] J. Leutgeb, J. Mager, and A. Rebhan, Hadronic light-by-light contribution to the muon $g - 2$ from holographic QCD with solved $U(1)_A$ problem, *Phys. Rev. D* **107**, 054021 (2023), [arXiv:2211.16562 \[hep-ph\]](#).
- [63] J. Mager, L. Cappiello, J. Leutgeb, and A. Rebhan, Longitudinal Short-Distance Constraints on Hadronic Light-by-Light Scattering and Tensor-Meson Contributions to the Muon $g - 2$, *Phys. Rev. Lett.* **135**, 091901 (2025), [arXiv:2501.19293 \[hep-ph\]](#).
- [64] P. Colangelo, F. Giannuzzi, and S. Nicotri, Hadronic light-by-light scattering contributions to $(g - 2)_\mu$ from axial-vector and tensor mesons in the holographic soft-wall model, *Phys. Rev. D* **109**, 094036 (2024), [arXiv:2402.07579 \[hep-ph\]](#).

- [65] L. Cappiello, O. Catà, and G. D’Ambrosio, Scalar resonances in the hadronic light-by-light contribution to the muon ($g-2$), *Phys. Rev. D* **105**, 056020 (2022), [arXiv:2110.05962 \[hep-ph\]](#).
- [66] L. Cappiello, O. Catà, G. D’Ambrosio, D. Greynat, and A. Iyer, Axial-vector and pseudoscalar mesons in the hadronic light-by-light contribution to the muon ($g-2$), *Phys. Rev. D* **102**, 016009 (2020), [arXiv:1912.02779 \[hep-ph\]](#).
- [67] L. Cappiello, J. Leutgeb, J. Mager, and A. Rebhan, Tensor meson transition form factors in holographic QCD and the muon $g-2$, *JHEP* **07**, 033, [arXiv:2501.09699 \[hep-ph\]](#).
- [68] L.-X. Cui, Z. Fang, and Y.-L. Wu, Infrared-Improved Soft-wall AdS/QCD Model for Mesons, *Eur. Phys. J. C* **76**, 22 (2016), [arXiv:1310.6487 \[hep-ph\]](#).
- [69] Z. Fang, Y.-L. Wu, and L. Zhang, Chiral phase transition and meson spectrum in improved soft-wall AdS/QCD, *Phys. Lett. B* **762**, 86 (2016), [arXiv:1604.02571 \[hep-ph\]](#).
- [70] Z. Fang, Y.-L. Wu, and L. Zhang, Octet meson spectra and chiral phase diagram in the improved soft-wall AdS/QCD model, *Phys. Rev. D* **100**, 054008 (2019), [arXiv:1904.04695 \[hep-ph\]](#).
- [71] P. Colangelo, F. De Fazio, F. Giannuzzi, F. Jugeau, and S. Nicotri, Light scalar mesons in the soft-wall model of AdS/QCD, *Phys. Rev. D* **78**, 055009 (2008), [arXiv:0807.1054 \[hep-ph\]](#).
- [72] J. Leutgeb, A. Rebhan, and M. Stadlbauer, Hadronic vacuum polarization contribution to the muon $g-2$ in holographic QCD, *Phys. Rev. D* **105**, 094032 (2022), [arXiv:2203.16508 \[hep-ph\]](#).
- [73] S. Navas *et al.* (Particle Data Group), Review of particle physics, *Phys. Rev. D* **110**, 030001 (2024).
- [74] T. Blum, Lattice calculation of the lowest order hadronic contribution to the muon anomalous magnetic moment, *Phys. Rev. Lett.* **91**, 052001 (2003), [arXiv:hep-lat/0212018](#).
- [75] C. Aubin and T. Blum, Calculating the hadronic vacuum polarization and leading hadronic contribution to the muon anomalous magnetic moment with improved staggered quarks, *Phys. Rev. D* **75**, 114502 (2007), [arXiv:hep-lat/0608011](#).
- [76] D. K. Hong, D. Kim, and S. Matsuzaki, Holographic calculation of hadronic contributions to muon $g-2$, *Phys. Rev. D* **81**, 073005 (2010), [arXiv:0911.0560 \[hep-ph\]](#).
- [77] H. R. Grigoryan and A. V. Radyushkin, Structure of vector mesons in holographic model with linear confinement, *Phys. Rev. D* **76**, 095007 (2007), [arXiv:0706.1543 \[hep-ph\]](#).
- [78] K. Ghoroku, N. Maru, M. Tachibana, and M. Yahiro, Holographic model for hadrons in deformed AdS(5) background, *Phys. Lett. B* **633**, 602 (2006), [arXiv:hep-ph/0510334](#).
- [79] R. Casero, E. Kiritsis, and A. Paredes, Chiral symmetry breaking as open string tachyon condensation, *Nucl. Phys. B* **787**, 98 (2007), [arXiv:hep-th/0702155](#).
- [80] I. Iatrakis, E. Kiritsis, and A. Paredes, An AdS/QCD model from Sen’s tachyon action, *Phys. Rev. D* **81**, 115004 (2010), [arXiv:1003.2377 \[hep-ph\]](#).
- [81] I. Iatrakis, E. Kiritsis, and A. Paredes, An AdS/QCD model from tachyon condensation: II, *JHEP* **11**, 123, [arXiv:1010.1364 \[hep-ph\]](#).
- [82] J. F. Donoghue, E. Golowich, and B. R. Holstein, *Dynamics of the Standard Model*, 2nd ed., Cambridge Monographs on Particle Physics, Nuclear Physics and Cosmology (Cambridge University Press, 2014).
- [83] M. Davier, A. Hoecker, B. Malaescu, and Z. Zhang, A new evaluation of the hadronic vacuum polarisation contributions to the muon anomalous magnetic moment and to $\alpha(m_Z^2)$, *Eur. Phys. J. C* **80**, 241 (2020), [Erratum: *Eur.Phys.J.C* 80, 410 (2020)], [arXiv:1908.00921 \[hep-ph\]](#).

- [84] H. R. Grigoryan and A. V. Radyushkin, Pion form-factor in chiral limit of hard-wall AdS/QCD model, *Phys. Rev. D* **76**, 115007 (2007), [arXiv:0709.0500 \[hep-ph\]](#).
- [85] H. J. Kwee and R. F. Lebed, Pion form-factors in holographic QCD, *JHEP* **01**, 027, [arXiv:0708.4054 \[hep-ph\]](#).
- [86] H. R. Grigoryan and A. V. Radyushkin, Anomalous Form Factor of the Neutral Pion in Extended AdS/QCD Model with Chern-Simons Term, *Phys. Rev. D* **77**, 115024 (2008), [arXiv:0803.1143 \[hep-ph\]](#).
- [87] F. Zuo and T. Huang, Photon-to-pion transition form factor and pion distribution amplitude from holographic QCD, *Eur. Phys. J. C* **72**, 1813 (2012), [arXiv:1105.6008 \[hep-ph\]](#).
- [88] S. J. Brodsky, F.-G. Cao, and G. F. de Teramond, Meson Transition Form Factors in Light-Front Holographic QCD, *Phys. Rev. D* **84**, 075012 (2011), [arXiv:1105.3999 \[hep-ph\]](#).
- [89] P. Colangelo, F. Giannuzzi, and S. Nicotri, π^0 , η , η' two-photon transition form factors in the holographic soft-wall model and contributions to $(g - 2)_\mu$, *Phys. Lett. B* **840**, 137878 (2023), [arXiv:2301.06456 \[hep-ph\]](#).
- [90] G. P. Lepage and S. J. Brodsky, Exclusive Processes in Perturbative Quantum Chromodynamics, *Phys. Rev. D* **22**, 2157 (1980).
- [91] H. J. Behrend *et al.* (CELLO), A Measurement of the π^0 , eta and eta-prime electromagnetic form-factors, *Z. Phys. C* **49**, 401 (1991).
- [92] J. Gronberg *et al.* (CLEO), Measurements of the meson - photon transition form-factors of light pseudoscalar mesons at large momentum transfer, *Phys. Rev. D* **57**, 33 (1998), [arXiv:hep-ex/9707031](#).
- [93] B. Aubert *et al.* (BaBar), Measurement of the $\gamma\gamma^* \rightarrow \pi^0$ transition form factor, *Phys. Rev. D* **80**, 052002 (2009), [arXiv:0905.4778 \[hep-ex\]](#).
- [94] S. Uehara *et al.* (Belle), Measurement of $\gamma\gamma^* \rightarrow \pi^0$ transition form factor at Belle, *Phys. Rev. D* **86**, 092007 (2012), [arXiv:1205.3249 \[hep-ex\]](#).
- [95] A. Nyffeler, Precision of a data-driven estimate of hadronic light-by-light scattering in the muon $g - 2$: Pseudoscalar-pole contribution, *Phys. Rev. D* **94**, 053006 (2016), [arXiv:1602.03398 \[hep-ph\]](#).
- [96] A. Gérardin, W. E. A. Verplanke, G. Wang, Z. Fodor, J. N. Guenther, L. Lellouch, K. K. Szabo, and L. Varnhorst, Lattice calculation of the π^0 , η and η' transition form factors and the hadronic light-by-light contribution to the muon $g - 2$, *Phys. Rev. D* **111**, 054511 (2025), [arXiv:2305.04570 \[hep-lat\]](#).
- [97] A. Gérardin, H. B. Meyer, and A. Nyffeler, Lattice calculation of the pion transition form factor with $N_f = 2 + 1$ Wilson quarks, *Phys. Rev. D* **100**, 034520 (2019), [arXiv:1903.09471 \[hep-lat\]](#).
- [98] M. Hoferichter, B.-L. Hoid, B. Kubis, S. Leupold, and S. P. Schneider, Pion-pole contribution to hadronic light-by-light scattering in the anomalous magnetic moment of the muon, *Phys. Rev. Lett.* **121**, 112002 (2018), [arXiv:1805.01471 \[hep-ph\]](#).
- [99] P. Masjuan and P. Sanchez-Puertas, Pseudoscalar-pole contribution to the $(g_\mu - 2)$: a rational approach, *Phys. Rev. D* **95**, 054026 (2017), [arXiv:1701.05829 \[hep-ph\]](#).
- [100] J. Leutgeb, J. Mager, and A. Rebhan, Divergences in the hadronic light-by-light amplitude of the holographic soft-wall model, (2025), [arXiv:2511.11797 \[hep-ph\]](#).